PHYSICAL REVIEW B **81**, 085434 (2010)

Superatom orbitals of $Sc_3N@C_{80}$ and their intermolecular hybridization on Cu(110)-(2×1)-O surface

Tian Huang,[1] Jin Zhao,[1] Min Feng,[1] Hrvoje Petek,[1,*] Shangfeng Yang,[2,3] and Lothar Dunsch[2]
[1]*Department of Physics and Astronomy, Petersen Institute of NanoScience and Engineering, University of Pittsburgh, Pittsburgh, Pennsylvania 15213, USA*
[2]*Department of Electrochemistry and Conducting Polymers, Leibniz-Institute for Solid State and Materials Research (IFW), Dresden, Germany*
[3]*Hefei National Laboratory for Physical Sciences at Microscale and Department of Materials Science and Engineering, University of Science and Technology of China (USTC), Hefei 230026, China*
(Received 25 November 2009; published 24 February 2010)

We investigate the electronic structure of an endohedral fullerene, $Sc_3N@C_{80}$, chemisorbed on Cu(110)-(2×1)-O surface by scanning tunneling microscopy and density-functional theory. Scanning tunneling microscopy and spectroscopy identify a series of delocalized atomlike superatom molecular orbitals (SAMOs) in the $Sc_3N@C_{80}$ and its aggregates. By contrast to C_{60}, the encapsulated Sc_3N cluster in $Sc_3N@C_{80}$ distorts the nearly-spherical central potential of the carbon cage, imparting an asymmetric spatial distribution to the SAMOs. When $Sc_3N@C_{80}$ molecules form dimers and trimers, however, the strong intermolecular hybridization results in highly symmetric hybridized SAMOs with clear bonding and antibonding characteristics. The electronic-structure calculations on $Sc_3N@C_{80}$ and its aggregates confirm the existence of SAMOs and reproduce their hybridization as observed in the experiment.

DOI: 10.1103/PhysRevB.81.085434 PACS number(s): 73.22.−f

I. INTRODUCTION

Following the discovery of C_{60} two decades ago, fullerenes have been studied extensively as promising materials for applications in molecular electronics and optoelectronics.[1–9] In a fullerene assembly, such as one-dimensional (1D) wire, two-dimensional (2D) quantum well, and three-dimensional crystal, the charge transport through the assembly is governed by the π-π stacking, which defines the intermolecular wave-function overlap,[10–14] similar to other molecular solids that are held together by van der Waals forces.[15,16]

In a recent scanning tunneling microscopy (STM) and density-functional theory (DFT) studies of chemisorbed C_{60} molecules on copper surfaces, however, we discovered a new paradigm for the intermolecular hybridization among hollow molecules.[17–19] Considering the σ and π molecular orbitals as the $n=1$ and 2 solutions of the central potential of the hollow C atom shell, the next higher $n=3$ or δ states could provide the requisite intermolecular wave-function overlap to achieve nearly-free-electron (NFE)-like band delocalization.[20,21] Because the δ orbitals were characterized by diffuse atomlike spatial distributions in STM experiments and DFT calculations, we have dubbed them the superatom molecular orbitals (SAMOs).[17] By contrast to the σ and π orbitals of fullerenes, which are highly degenerate and tightly bound to individual C atoms, the SAMOs are more loosely bound to the screening potential of the hollow molecular cage. Their radial and angular distributions can be described by the spherical harmonic functions similar to the s, p, and d orbitals of H atom. The SAMOs extend spatially further from the C atom shell than the more tightly bound π orbitals and can hybridize in a C_{60} dimer like the s and p orbitals of hydrogen atoms into a H_2-like superatom molecule; in extended 1D and 2D C_{60} assemblies, SAMOs hybridize into s-electron metal-like NFE bands.[17,22] Because SAMOs originate from the binding of electrons to the central potential of their screening charge, they are a general property of hollow molecules.[17]

Whether or not SAMO-mediated transport is feasible in fullerene quantum structures and solids depends on the SAMO energy with respect to the π-orbital-derived highest occupied molecular orbital (HOMO) and lowest unoccupied molecular orbital (LUMO) states. For example, the calculated energy of the lowest energy s-SAMO of C_{60} is 3.28 eV above the LUMO. A time-resolved two-photon photoemission study on the C_{60}/Au(111) surface showed that electrons excited to a 2D NFE quantum well formed by hybridization of s-SAMO decay on the femtosecond time scale,[22] possibly to the lower-lying LUMO states. While such short lifetime impedes the use of C_{60} in practical SAMO-mediated charge transport, a strategy for tuning the energy of the SAMOs by endohedral doping with metal atoms has been proposed.[18]

Endohedral fullerenes have been a particularly attractive subject for research because of their unique properties associated with the interaction and charge transfer between the encapsulated metal atoms or clusters and the carbon cage.[23–27] The family of endohedral fullerenes containing M_3N clusters, where M is a Group III metal atom, have been of interest because they might exhibit the violation of the isolated pentagon rule for the stability of fullerenes. They are predicted to enhance electron transmission through single-molecule junctions, and exhibit M-dependent cluster rotation at room temperature.[25,28,29] In this work, we studied the electronic structure of an endohedral fullerene, $Sc_3N@C_{80}$, adsorbed on Cu(110)-O surface by LT-STM and DFT calculations (1) to verify the universal nature of the SAMOs and (2) to explore how the endohedral doping of an endohedral fullerene affects the energy, spatial distribution, and intermolecular hybridization of its SAMOs.

II. EXPERIMENTAL SECTION

The experiments were performed with an Omicron LT-STM system composed of two connected ultrahigh-vacuum chambers. As in our previous study, we employed a partially oxidized single-crystal Cu(110) substrate.[30] The substrate was cleaned by Ar^+-ion (600 V) sputtering and annealing cycles. The clean Cu(110) surface was dosed with 6.8 L of high-purity O_2 at 520 K to form a partially oxidized Cu(110)-(2×1)-O surface.[30] The $Sc_3N@C_{80}$ sample used in this study was prepared and purified as described elsewhere.[25,32] A submonolayer of $Sc_3N@C_{80}$ molecules was deposited by thermal evaporation at 670 K on the Cu(110)-(2×1)-O surface. During the deposition, the substrate was kept at room temperature and the chamber pressure was below 1×10^{-8} Torr. The sample was then transferred to the STM chamber with a base pressure less than 3×10^{-11} Torr, and cooled down to 78 K for experimental measurements. Constant current STM images and distance-voltage (z-V) spectra were recorded with an electrochemically etched tungsten tip, which was prepared by field emission as well as *in situ* cleaning treatment. dI/dV images giving the local density of states (LDOS) at specific bias voltages were measured by adding an ac modulation of 15 mV (rms) at 693 Hz to the junction bias (sample potential referenced to the tip) and demodulating the tunneling current with a lock-in amplifier.

III. THEORETICAL METHODS

As in our previous calculations on C_{60} SAMOs, we performed plane-wave basis set DFT electronic-structure calculations using the generalized gradient approximation with the PBE (Ref. 33) functional as implemented in the Vienna *ab initio* simulation package.[34–36] The projector augmented wave method was used to describe the electron-ion interaction.[37] The plane-wave basis set cut-off energy was set to 500 eV. For Sc atom, the $1s$-$2p$ were treated as core orbitals. For the isolated $Sc_3N@C_{80}$ molecule calculation, we used a cubic unit cell with dimension $a=30$ Å. For $Sc_3N@C_{80}$ dimer and trimer, we used larger unit cells of $40\times30\times30$ and $40\times40\times30$ Å, respectively.

IV. RESULTS AND DISCUSSION

A. SAMOs of isolated $Sc_3N@C_{80}$ molecules

$Sc_3N@C_{80}$ molecules contain a planar triangular nitride Sc_3N cluster with its C_3 rotation axis coinciding with that of the I_h symmetry C_{80} cage[29,31] [Fig. 1(a)]. The partially oxidized Cu(110)-(2×1)-O surface is composed of >100-nm-wide (2×1)-O domains separated by the 0.76-nm-wide linear gaps of bare Cu running along the ⟨001⟩ direction, as shown in Figs. 1(b) and 1(c). After deposition onto the Cu(110)-O substrate $Sc_3N@C_{80}$ molecules are found adsorbed both on the (2×1)-O domains and in the Cu troughs. Besides the individual monomers, $Sc_3N@C_{80}$ molecules also aggregate into small structures such as dimers and trimers [Fig. 1(d)]. According to dI/dV spectroscopy, which will be discussed in a separate publication, the LUMO

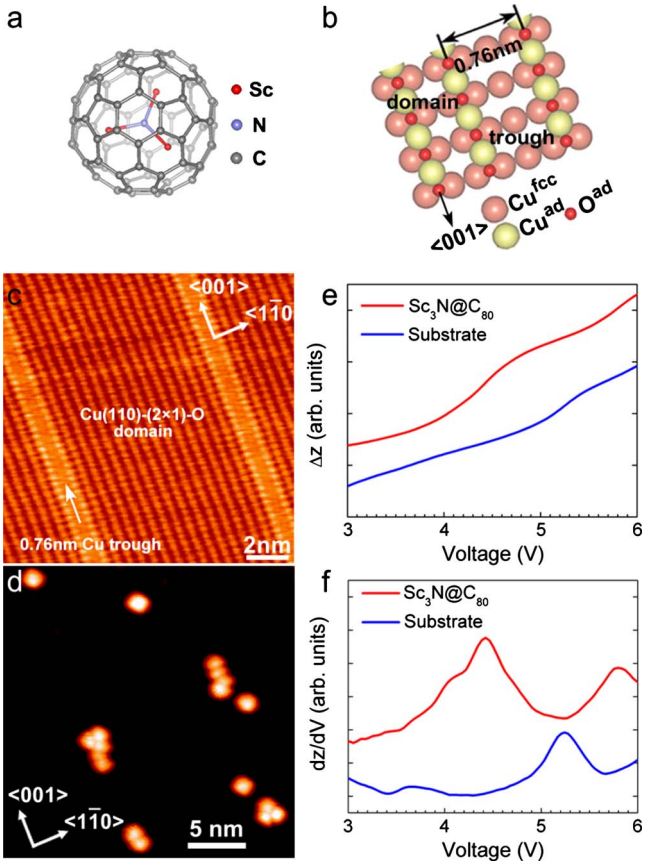

FIG. 1. (Color online) (a) Molecular model of $Sc_3N@C_{80}$. (b) Schematic model of the partially oxidized Cu(110)-(2×1)-O surface. (c) High-resolution STM topographic image of the partially oxidized Cu(110)-(2×1)-O surface showing both the 0.76 nm Cu troughs and the (2×1)-O domains. (d) STM image of $Sc_3N@C_{80}$ adsorbed on Cu(110)-(2×1)-O surface. The tunneling conditions are $V_{bias}=0.5$ V and $I_{setpoint}=400$ pA for (a), and $V_{bias}=0.79$ V and $I_{setpoint}=150$ pA for (d). (e) z-V spectra for $Sc_3N@C_{80}$ and Cu(110)-(2×1)-O domain measured with initial tunneling conditions of $V_{bias}=1.0$ V and $I_{setpoint}=200$ pA. (f) Numerical derivative of (e). The curves are displaced with respect to each other for clarity.

of $Sc_3N@C_{80}$ lies at ~0.5 V above the Fermi level (E_F). To identify the SAMOs, which appear above 3.5 V for C_{60}, we recorded distance-voltage (z-V) scans by ramping the tip-sample bias while keeping the current constant and feedback loop engaged. The slope of the z-V curve changes whenever a resonant tunneling channel becomes available to increase the tunneling probability. Compared with the conventional I-V spectroscopy, the z-V method prevents the sample or tip damage due to the high tunneling current at high bias voltage.[38,39] Figure 1(e) shows z-V spectra measured on an adsorbed $Sc_3N@C_{80}$ monomer as well as on the (2×1)-O domain. Each curve is an average of 10–20 scans measured at the center of the same molecule. The energetic positions for opening of the tunneling channels for $Sc_3N@C_{80}$ molecule and the substrate are apparently different. This difference in the resonances can be seen more clearly in the numerical derivatives of the z-V curves (dz/dV vs V), as shown in Fig. 1(f). The characteristic resonance at 3.7 V of the

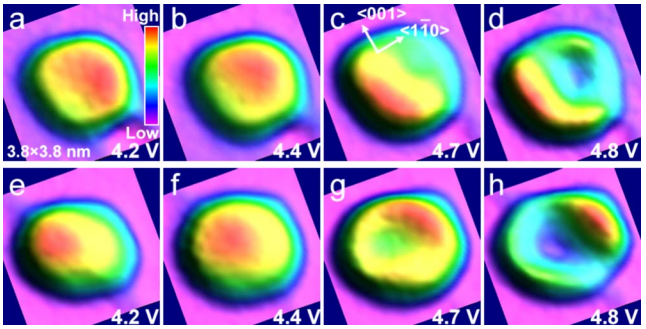

FIG. 2. (Color online) [(a)–(d)] dI/dV mapping showing the LDOS of SAMOs of an individual $Sc_3N@C_{80}$ molecule at different energies. [(e)–(h)] dI/dV mapping of the SAMOs of another $Sc_3N@C_{80}$ molecule showing different spatial distributions. The measurement bias voltages are indicated in the figures; the tunneling current $I_{setpoint}$ is 200 pA.

substrate, which corresponds to a surface state of Cu-O atom chain, disappears above the $Sc_3N@C_{80}$ molecule; instead there appears a new peak with a maximum at ~4.4 V and a shoulder at ~4 V.

To find out whether these resonances correspond to the SAMOs of $Sc_3N@C_{80}$, we imaged their spatial distributions by recording the dI/dV images at different energies within the 4.4 V peak region in the dz/dV curve. Figures 2(a)–2(d) show dI/dV images taken between 4.2–4.8 V, in which the orbitals exhibit approximate monopolar and dipolar symmetries. Based on their diffuse spatial distributions, the orbitals are distinct from the more tightly bound π orbitals directed along the C-C bonds, such as have been observed for C_{60} molecules,[40,41] and from lower bias $Sc_3N@C_{80}$, images, which show strong and asymmetric LDOS localization within a molecule on account of the tunneling pathways mediated by the endohedral cluster. Unlike C_{60}, however, the high DOS of the Sc_3N cluster appears to obscure specific resonances associated with the π^* orbitals in the dz/dV spectra. In addition to their diffuse LDOS, SAMOs exhibit strong intermolecular hybridization when two or more molecules aggregate into clusters, which will be discussed in the next section. The diffuse nature and intermolecular hybridiztion leads us to conclude that the images in Figs. 2(a) and 2(b) correspond to the $m=0$ SAMOs (s- or p_z-like; m is the surface projection of the angular-momentum quantum number l), whereas Figs. 2(c) and 2(d) correspond to the $m=1$ SAMOs (p_x-/p_y-like).

The asymmetry of SAMOs could arise from the anisotropy of the substrate and the structure of the endohedral cluster within the fullerene cage. For adsorbed C_{60} molecules, the broken symmetry of space and the anisotropy of O/Cu(110) surface cause the degenerate p-SAMO to split into three spatially distinct orthogonal p_x-, p_y-, and p_z-SAMO's that extend along the $\langle 1\bar{1}0\rangle$, $\langle 001\rangle$, and $\langle 110\rangle$ directions, respectively. The p_z-SAMO of C_{60} further hybridizes with s-SAMO into a bonding (3.70 V) and an antibonding (4.15 V) pair, with orbital density pointing into and away from the surface.[17] In $Sc_3N@C_{80}$, the D_{3h} symmetry of Sc_3N cluster along with the anisotropy of the substrate mixes the p_x- and p_y-SAMO's, causing the resulting asymmetric orbitals to align with low-symmetry directions of the substrate [Figs. 2(c) and 2(d)]. While s- and p_z-SAMO's contribute to the monopolar symmetry in Figs. 2(a) and 2(b), we could not find distinct evidence of their intramolecular hybridization in the experimental images. Keeping in mind that the adsorption environments for $Sc_3N@C_{80}$ and C_{60} are the same, we believe that the properties of the SAMOs in $Sc_3N@C_{80}$ are influenced by the inclusion of the D_{3h} symmetry Sc_3N cluster, as well as the change in the cage size. The p_x- and p_y-SAMO's are likely to be nearly degenerate and to mix through the incompatible symmetry of the endohedral cluster and the substrate (we assume that for most molecules the cluster is nearly parallel to the surface plane,[28] as explained below). The endohedral cluster distorts the nearly-spherical central potential of the carbon cage leading to asymmetric SAMOs of the isolated molecules, as will be supported by our calculations.

Figures 2(e)–2(h) show the dI/dV images recorded on another $Sc_3N@C_{80}$ molecule, which confirm the existence of the $m=0$ and 1 SAMOs. While the $m=0$ SAMO is similar to the one in Figs. 2(a) and 2(b), the $m=1$ SAMOs have different distributions. It is possible that this variability in SAMO distributions originates from several factors including different molecular adsorption configurations of the C_{80} cage, the distribution in and possibly interconversion between several rotational isomer configurations of Sc_3N cluster, and presence of further isomeric structures associated with the orientation of the cluster C_3 axis with respect to the surface plane. The existence of such isomeric forms has been addressed in a recent STM and x-ray photoelectron diffraction study of $Dy_3N@C_{80}$ adsorbed on Cu(111) surface, where Treier *et al.*[28] found that the molecules form domains with the same orientation of the C_{80} cage, whereas the encapsulated cluster occupies at least two inequivalent orientations within the C_{80} cage. Based on the structural similarity of $Sc_3N@C_{80}$ and $Dy_3N@C_{80}$, it is therefore possible that the different orientation of the encapsulated Sc_3N cluster with respect to the carbon cage is responsible for the molecule-to-molecule differences in the LDOS of $m=1$ SAMOs. Because of their vague shapes, the classification of SAMO into distinct structures and analysis according to their statistical probability of appearance has not been attempted.

B. HYBRIDIZATION OF SAMO'S IN $Sc_3N@C_{80}$ CLUSTERS

Because SAMOs are more spatially diffuse than the σ and π orbitals of the fullerenes, we expect them to hybridize within a $Sc_3N@C_{80}$ molecular assembly, as we found for C_{60} molecules.[17] Therefore, we further investigated the electronic structures of $Sc_3N@C_{80}$ aggregates to investigate the nature of SAMO-mediated intermolecular hybridization.

1. Fullerene dimer

We start from the smallest cluster, i.e., $Sc_3N@C_{80}$ dimer. Many metal-containing endohedral fullerenes such as $Tb@C_{82}$,[42] $Nd@C_{82}$,[43] and $Y@C_{82}$[44] have a tendency to form dimers especially in the solid state. The dimerization has been explained by intermolecular interactions originating from a permanent dipole moment[43] or an unpaired electron[44]

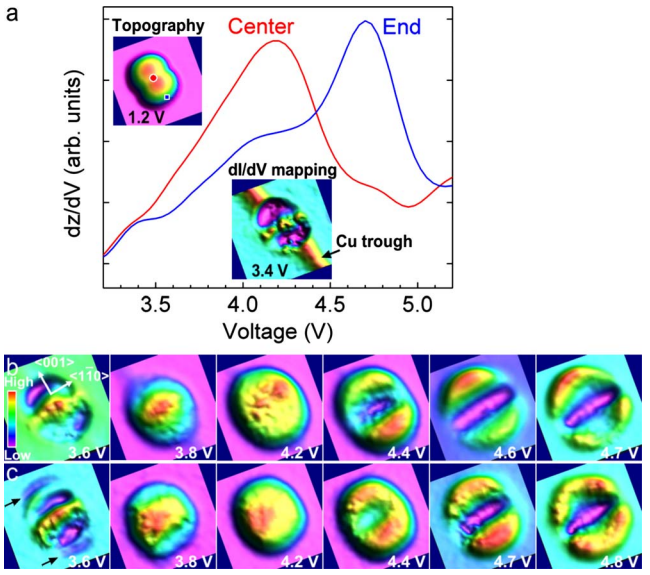

FIG. 3. (Color online) (a) dz/dV spectra measured at the center and an end of a $Sc_3N@C_{80}$ dimer. Top inset: STM topography of a dimer adsorbed on a 0.76 nm Cu trough; the red circle and blue square indicate the positions where the dz/dV spectra were recorded. Bottom inset: dI/dV image of the dimer recorded at 3.4 V showing the LDOS of the Cu trough. Imaging dimensions for both insets are 5.0×5.0 nm^2. [(b) and (c)] dI/dV mapping of the SAMOs in two different $Sc_3N@C_{80}$ dimers. SAMOs show typical bonding and antibonding characteristics originating from the strong hybridization between molecules. In (b) and (c) the dimers are adsorbed on a Cu trough and (2×1)-O domain, respectively. At 3.6 V, the dimer adsorbed on the (2×1)-O domain shows distinct LDOS at each end [black arrows in (c)], which is caused by scattering of surface state electrons of the substrate at adsorbed molecules. The measurement bias voltages are indicated in the figures; the tunneling current $I_{setpoint}$ is 200 pA, and the imaging size is 4.2×4.2 nm^2.

at the fullerene cage. In our experiment, $Sc_3N@C_{80}$ molecules are found forming dimers both on the (2×1)-O domains and the unoxidized 0.76-nm-wide Cu troughs. In both cases the dimers align along the $\langle001\rangle$ direction of the substrate and the SAMOs images are similar. Figure 3(a) shows the spatially resolved dz/dV spectra recorded at different tip positions along the dimer axis. The spectra reveal that the characteristic peak at ~4.4 V for $Sc_3N@C_{80}$ monomer splits into two peaks at 4.1 and 4.7 V peaks, in the case of a dimer. The intensity maxima occur at the center and the ends of the dimer, respectively, for the 4.1 and 4.7 V resonances. Figure 3(b) presents the dI/dV images in the 3.6–4.8 V range. The splitting of the 4.4 V peak of the monomer into a lower and higher energy resonances and the spatial distribution of the new states shown in Fig. 3(b) strongly suggest the intermolecular hybridization of the SAMOs into a bonding and antibonding pair of the dimer. The SAMO orbitals are only transiently occupied by tunneling electrons from the STM tip, and otherwise have no impact on the cohesion of a dimer, which is determined by the ground-state molecule-surface and molecule-molecule interactions.

The atomlike orbitals of $Sc_3N@C_{80}$ hybridize into molecular orbitals of dimers with σ and π symmetry bonding and antibonding characters, as would atomic orbitals of H atoms when combined into an H_2 molecule. Specifically, in the range from 3.6 to 4.2 V the hybridized orbitals exhibit the σ- and π-bonding characters, as judged by the accumulation of LDOS in the center of the dimer. A strong distinction between the σ- and π-bonds is not observed probably because of the approximate symmetry of the monomer orbitals and because both kinds of bonds contribute in the same energy interval. Between 4.4 and 4.6 V the orbitals acquire σ^* antibonding character, as judged by appearance of a node bisecting the dimer. Finally, at 4.7 V the hybridized orbitals show π^* antibonding character with an additional node along the dimer axis. Figure 3(c) shows the dI/dV images recorded on another $Sc_3N@C_{80}$ dimer. By contrast to the $Sc_3N@C_{80}$ monomers, for which the SAMO shape differs significantly from molecule-to-molecule, as we noted in the last section, the SAMOs of dimers have nearly-identical spatial distributions in all the recorded images. The consistent dimer orbital shape suggests that (i) it is dominated either by the intermolecular hybridization; (ii) it is independent of the Sc_3N cluster geometry; (iii) the cluster can rearrange continuously during the measurement; or (iv) the dimerization causes the adjacent molecules in a cluster to align into a specific conformation. We believe that the similarity arises mainly from the strong intermolecular hybridization. Compared with C_{60}, the hybridization-induced peak shift in dz/dV spectra of $Sc_3N@C_{80}$ dimer is much larger,[17] confirming the strong hybridization. According to the similarity of the images for dimers above Cu trough and (2×1)-O domains, we conclude that the density distribution is independent of the substrate and appears to be dominated by the intermolecular interaction.

2. Linear fullerene trimer

The hybridization of the SAMOs is further investigated for the $Sc_3N@C_{80}$ trimers. The 0.76 nm bare Cu troughs on the surface provide templates for the growth of linear trimers as shown in Fig. 4(a). The characteristic peak at 4.4 V for $Sc_3N@C_{80}$ monomer again splits into two peaks at 3.8 and 4.4 V, indicating formation of hybridized SAMOs of the trimer. The low-energy resonance has the intensity maximum at center of the trimer, whereas the high-energy one shows maxima at the ends.

Figures 4(b)–4(g) present the dI/dV LDOS images of the hybridized SAMOs of the trimer. Compared with the dimer, the two peaks shift down in energy, and the 3.8 V resonance is less localized within the aggregate than its counterpart for the dimer. The LDOS images in Figs. 4(b) and 4(c) show the bonding character, whereas Figs. 4(d)–4(g) show the antibonding character. The 4.2 and 4.5 V orbitals have one and two nodes, respectively, characteristic of the σ^* antibonding character, whereas the 4.7 and 4.8 V orbitals have additional nodes along and perpendicular to the trimer axis expected for the π^* antibonding character.

3. Triangular fullerene trimer

In addition to the linear $Sc_3N@C_{80}$ trimer, the intermolecular interaction also favors the formation of fullerene tri-

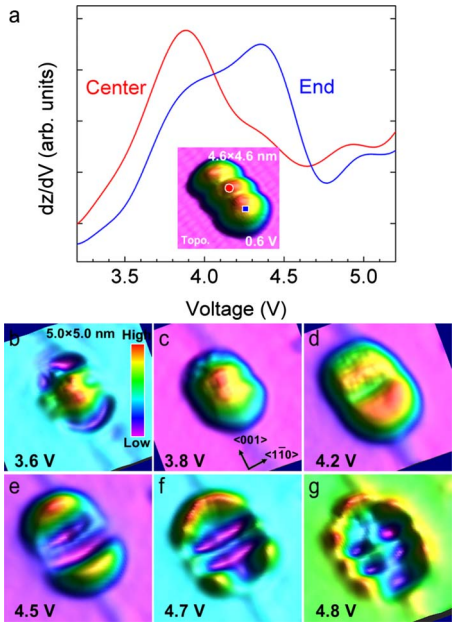

FIG. 4. (Color online) (a) dz/dV spectra measured at the center and the end of a linear $Sc_3N@C_{80}$ trimer adsorbed on a Cu trough. Inset: STM topography of a linear trimer; the red circle and blue square indicate the positions where the dz/dV spectra were recorded. [(b)–(g)] dI/dV mapping of the trimer at different energies revealing the intermolecular hybridization of the SAMOs. The measurement bias voltages are indicated within the figures; the tunneling current $I_{setpoint}$ is 200 pA.

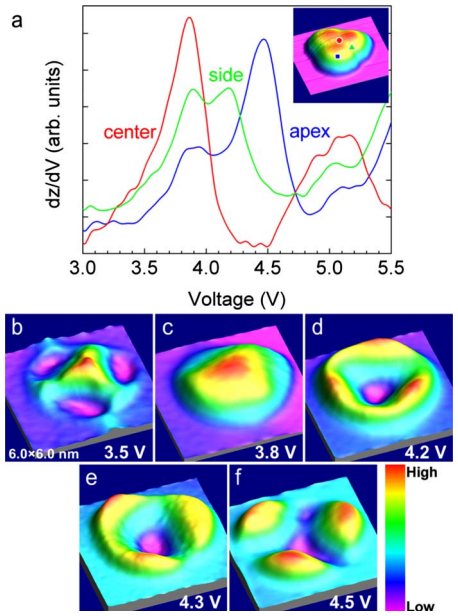

FIG. 5. (Color online) (a) dz/dV spectra measured at different positions of a triangular $Sc_3N@C_{80}$ trimer. Inset: STM topography of a trimer, where red circle, green triangle, and blue square indicate the positions where the dz/dV spectra were recorded. [(b)–(f)] dI/dV mapping of the triangular $Sc_3N@C_{80}$ trimer at different energies. The measurement bias voltages are indicated in the figures; the tunneling current $I_{setpoint}$ is 200 pA.

mers with an equilateral triangle shape, as shown in the inset of Fig. 5. Within this trimer, two molecules adsorb on the Cu trough while the third one is on the (2×1)-O domain. Despite experiencing different molecule-surface interactions, the hybridized SAMO orbitals of the three molecules appear to be electronically identical. The dz/dV spectra recorded at different positions [Fig. 5(a)] show the existence of three types of hybridized SAMOs, which have different spatial distributions. From the corresponding LDOS images in Figs. 5(b)–5(f), it is clear that the 3.5–3.8 V resonance [Figs. 5(b) and 5(c)] has a bonding character with its density mainly in the gaps between the neighboring molecules and the density maximum at the center of the trimer. The 4.2 V resonance [Fig. 5(d)] has LDOS maxima at the center of each side of the three sides of the triangle. The 4.3–4.5 V region, however, shows antibonding character, where the hybridized orbital is located mainly at the three corners of the triangle. It is notable that despite the asymmetric spatial distribution of the single molecular SAMOs, the hybridized SAMOs of the trimer show a perfect threefold symmetry. This suggests the intermolecular hybridization within the fullerene trimer is sufficiently strong to obliterate distinct character of the component molecules arising from the adsorption on Cu vs Cu-O domains or possible differences in the internal conformations of the Sc_3N cluster.

C. DFT CALCULATIONS OF THE SAMO'S OF $Sc_3N@C_{80}$

Figure 6(a) shows the calculated DOS of an isolated $Sc_3N@C_{80}$ molecule. The band gap between HOMO and LUMO of 1.48 eV agrees with previous calculations.[29] The delocalized DOS corresponding to *s*-SAMO's appears at 3.29 eV above LUMO, with the *p*- and *d*-SAMO's appearing at 3.44 and 3.59 eV, respectively. The energy difference between SAMOs of $Sc_3N@C_{80}$ is smaller than for C_{60}, most likely because of their interaction with the unoccupied orbitals of the internal cluster. In Fig. 6(b), we show the calculated *s*- and *p*-SAMO probability densities for $Sc_3N@C_{80}$ molecule oriented with a hexagon facing up, which is the preferred orientation for $Dy_3N@C_{80}$ adsorbed on Cu(111) surface according to the photoemission diffraction.[28] In this orientation the C_{80} cage attaches the surface with a hexagon,

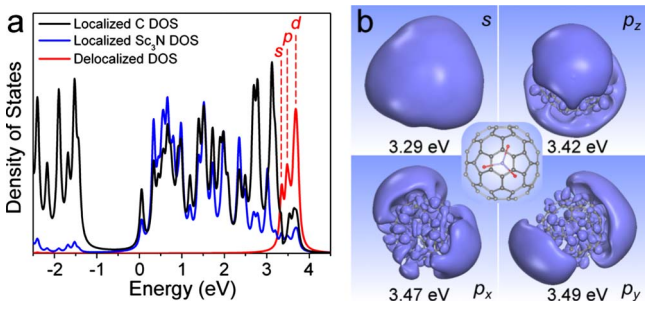

FIG. 6. (Color online) (a) Calculated DOS of an isolated $Sc_3N@C_{80}$ molecule analyzed into components that are localized on the carbon cage and Sc_3N cluster, and delocalized from the atomic centers. The energy of LUMO is set to zero. (b) Calculated *s*- and *p*-SAMO wave functions for an isolated $Sc_3N@C_{80}$ molecule. The energy is relative to LUMO. The inset shows the top view of the molecular structure.

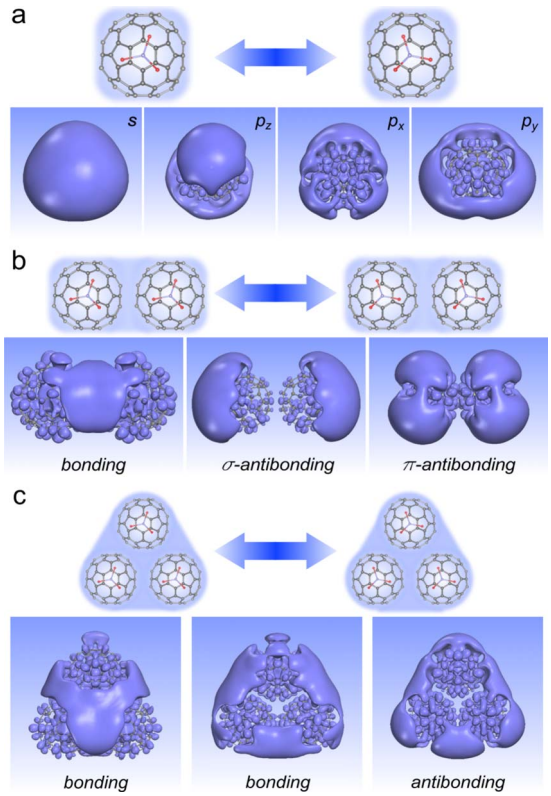

FIG. 7. (Color online) The calculated SAMO probability densities obtained by adding the distributions of two $Sc_3N@C_{80}$ molecules with different Sc_3N cluster azimuths, as shown in the molecular structures. (a) monomer; (b) dimer; and (c) trimer.

which causes the planar Sc_3N cluster to be slightly tilted relative to the surface. Although there is no guarantee that the C_{80} cage adopts the same orientation on Cu(110)-O surface, because we have no other information, we assume this orientation in displaying our theoretical results. It can be seen that the *s*-SAMO follows the triangular shape of the Sc_3N cluster. The *p*-SAMO's are also distorted from the ideal spherical harmonic symmetry by the endohedral Sc_3N cluster, in agreement with experiment. The triangular cluster causes mixing of the *p*- and *d*-SAMO's, which is reflected in the asymmetric shapes and the overlap of the *p*- and *d*-SAMO energy ranges.

The Sc_3N cluster can adopt ten equivalent orientations within the C_{80} cage by aligning its C_3 axis to ten different C_3 axes of the C_{80} cage. For each orientation, the Sc_3N cluster can occupy four equivalent positions with different azimuths corresponding to rotation about its C_3 axis. The energy barrier for rotation with respect to the C_3 axis of the cluster is calculated to be around 90 meV.[29] At 78 K we expect the thermal rotation of the cluster to be frozen out, but nevertheless, isomerization may be possible through excitation by inelastic electron tunneling. Therefore, during the STM measurements, the $Sc_3N@C_{80}$ may isomerize between the two configurations through the Sc_3N cluster rotation, as shown in Fig. 7(a). Because the LDOS images obtained in the STM measurements are likely to have contributions from two or more Sc_3N azimuths through interconversion by the tunneling electrons, we have represented the probability density distributions of the monomer, dimer, and triangular trimer by adding the distributions of two $Sc_3N@C_{80}$ molecules with different Sc_3N cluster azimuths, as shown in Figs. 7(b) and 7(c). The SAMOs of $Sc_3N@C_{80}$ dimers and trimers clearly show the general bonding and antibonding characteristics and high symmetry that would be expected for atoms when combining into similar structures. Compared with C_{60}, the pattern of molecular bonding and antibonding orbitals of $Sc_3N@C_{80}$ aggregates is less distinct. The blurring of the distinct atomic character of SAMOs of $Sc_3N@C_{80}$ molecules can be attributed to the mixing of the *s*-, *p*- and *d*-SAMO character through the influence of the endohedral cluster, which lacks the icosahedral symmetry of the C_{80} fullerene cage.

V. DISCUSSION

Whereas the radial quantum number $n=3$ orbitals of C_{60} molecules have been reported in several theoretical calculations that treated the fullerene cage as a hollow conducting sphere,[20,21] they were first imaged by Feng *et al.*[17] in LT-STM measurements at bias voltages above 3.5 V. Their simple spherical harmonic LDOS distributions were attributed to the central exchange-correlation potential within the hollow C_{60} core. In that and a subsequent publication, Zhao *et al.*[18] argued that doping fullerenes with endohedral atoms could be used as a strategy for affecting the energy and intermolecular hybridization of SAMOs. In the present work, we have (i) demonstrated the existence of SAMOs for $Sc_3N@C_{80}$ monomers; (ii) imaged their hybridization into dimeric and trimeric aggregates; and (iii) demonstrated that endohedral atoms and cluster can influence the properties of SAMOs.

The Sc_3N cluster within the fullerene cage affects the symmetry and energy of the resulting SAMOs. The D_{3h} symmetry of the cluster and the anisotropy of Cu(110)-O surface both serve to mix SAMOs of different orbital quantum number *l*. The asymmetric monomer images therefore reflect the combined effects of the azimuthal orientation of the internal cluster, and the angle of the cluster with respect to the ⟨001⟩ direction of the bare Cu domains. The cluster also affects the energies of SAMOs. The *s*-SAMO, which has the maximum probability density for C_{60} molecules at the center of the fullerene cage, is destabilized by the Pauli exclusion by the central N atom. Zhao *et al.*[18] demonstrated that metal atoms in the center of C_{60} cage lower the energy of *s*-SAMO through the hybridization between the atom and superatom orbitals of *s* symmetry. The situation, however, is somewhat different for the *p*- and *d*-SAMO's, which have nodes bisecting the cage; in the case of $Sc_3N@C_{80}$, their energies are reduced with respect to those of C_{60}. This stabilization may be a consequence of hybridization of the orbitals of the metal atoms of the endohedral cluster with the *p*- and *d*-SAMO's, which may be more effective than in the case when metal atoms occupy the center of the fullerene core.

In addition to providing new information on the intramolecular hybridization of SAMOs, our study shows interesting aspects of the intermolecular hybridization for $Sc_3N@C_{80}$ dimers and trimers. Considering the pronounced changes in

the dz/dV spectra as the $Sc_3N@C_{80}$ aggregation increases from monomers to dimers and trimers, the intermolecular hybridization is significantly stronger for $Sc_3N@C_{80}$ as compared with C_{60}. The stronger hybridization of $Sc_3N@C_{80}$ aggregates may stem from the presence of the electronegative N atom in the center. Because of Pauli exclusion, the central N atom expels some of the SAMO density to the exterior of the fullerene cage. This external density may be responsible for the enhanced hybridization. The hybridized orbitals of the linear and triangular fullerene trimers are the origin of the nearly-free-electron-like quantum wire and quantum well band formation that we reported for C_{60} molecules on copper surfaces.[17]

VI. CONCLUSIONS

In summary, by LT-STM experiments and DFT electronic-structure calculations, we have shown that the endohedral cluster fullerene $Sc_3N@C_{80}$ has a series of delocalized superatom molecular orbitals, which originate from the central exchange-correlation potential. Our findings substantiate our previous hypothesis that the SAMOs are universal characteristic of hollow molecules.[17,18] The SAMOs of $Sc_3N@C_{80}$ show strong atomic-orbital-like hybridization into delocalized states upon the formation dimers and trimers. Although SAMOs of single $Sc_3N@C_{80}$ molecules show asymmetry that can be attributed to the structure of the internal cluster, the orbitals formed by SAMO hybridization within two or three molecule aggregates exhibit higher symmetry with minimal variability between different samples, indicating that the LDOS distributions are dominated by strong intermolecular interactions. The energies and spatial distributions of SAMOs of $Sc_3N@C_{80}$ molecules are significantly different from those of C_{60}, demonstrating the feasibility of influencing the properties of SAMOs by the size of the carbon cage and endohedral inclusions. The large variety of fullerene cages and internal clusters offers the possibility designing endohedral fullerenes with distinct SAMO-derived properties that may be useful for electronic and optical applications of molecular materials.

ACKNOWLEDGMENTS

This work was funded by the W. M. Keck Foundation and Division of Chemical Sciences, Geosciences, and Biosciences, Office of Basic Energy Sciences of the U.S. Department of Energy through Grant No. DE-FG02-09ER16056. The calculations were performed in the Environmental Molecular Sciences Laboratory at the Pacific Northwest National Laboratory, a user facility sponsored by the DOE Office of Biological and Environmental Research. The authors acknowledge insightful discussions with T. Seideman, P. Echenique, V. Silkin, and E. Chulkov. We thank A. A. Popov (IFW Dresden) for helpful comments.

*Author to whom correspondence should be addressed; petek@pitt.edu

[1] L. Sanchez, R. Otero, J. M. Gallego, R. Miranda, and N. Martin, Chem. Rev. (Washington, D.C.) **109**, 2081 (2009).
[2] R. B. Ross, C. M. Cardona, D. M. Guldi, S. G. Sankaranarayanan, M. O. Reese, N. Kopidakis, J. Peet, B. Walker, G. C. Bazan, E. Van Keuren, B. C. Holloway, and M. Drees, Nature Mater. **8**, 208 (2009).
[3] D. M. Guldi, B. M. Illescas, C. M. Atienza, M. Wielopolskia, and N. Martin, Chem. Soc. Rev. **38**, 1587 (2009).
[4] Y. Y. Wang, R. Yamachika, A. Wachowiak, M. Grobis, and M. F. Crommie, Nature Mater. **7**, 194 (2008).
[5] P. W. M. Blom, V. D. Mihailetchi, L. J. A. Koster, and D. E. Markov, Adv. Mater. **19**, 1551 (2007).
[6] L. Forro and L. Mihaly, Rep. Prog. Phys. **64**, 649 (2001).
[7] C. Joachim, J. K. Gimzewski, and A. Aviram, Nature (London) **408**, 541 (2000).
[8] M. Prato, J. Mater. Chem. **7**, 1097 (1997).
[9] O. Gunnarsson, Rev. Mod. Phys. **69**, 575 (1997).
[10] W. W. Pai, C. L. Hsu, M. C. Lin, K. C. Lin, and T. B. Tang, Phys. Rev. B **69**, 125405 (2004).
[11] C. Silien, N. A. Pradhan, W. Ho, and P. A. Thiry, Phys. Rev. B **69**, 115434 (2004).
[12] L. L. Wang and H. P. Cheng, Phys. Rev. B **69**, 165404 (2004).
[13] K. D. Tsuei, J. Y. Yuh, C. T. Tzeng, R. Y. Chu, S. C. Chung, and K. L. Tsang, Phys. Rev. B **56**, 15412 (1997).
[14] T. Hashizume, K. Motai, X. D. Wang, H. Shinohara, Y. Saito, Y. Maruyama, K. Ohno, Y. Kawazoe, Y. Nishina, H. W. Pickering, Y. Kuk, and T. Sakurai, Phys. Rev. Lett. **71**, 2959 (1993).
[15] F. S. Tautz, Prog. Surf. Sci. **82**, 479 (2007).
[16] V. Coropceanu, J. Cornil, D. A. da Silva, Y. Olivier, R. Silbey, and J. L. Bredas, Chem. Rev. (Washington, D.C.) **107**, 926 (2007).
[17] M. Feng, J. Zhao, and H. Petek, Science **320**, 359 (2008).
[18] J. Zhao, M. Feng, J. L. Yang, and H. Petek, ACS Nano **3**, 853 (2009).
[19] V. M. Silkin, J. Zhao, F. Guinea, E. V. Chulkov, P. M. Echenique, and H. Petek, Phys. Rev. B **80**, 121408 (2009).
[20] J. L. Martins, N. Troullier, and J. H. Weaver, Chem. Phys. Lett. **180**, 457 (1991).
[21] C. Yannouleas and U. Landman, Chem. Phys. Lett. **217**, 175 (1994).
[22] X. Y. Zhu, G. Dutton, D. P. Quinn, C. D. Lindstrom, N. E. Schultz, and D. G. Truhlar, Phys. Rev. B **74**, 241401(R) (2006).
[23] C. M. Cardona, A. Kitaygorodskiy, and L. Echegoyen, J. Am. Chem. Soc. **127**, 10448 (2005).
[24] C. M. Cardona, B. Elliott, and L. Echegoyen, J. Am. Chem. Soc. **128**, 6480 (2006).
[25] L. Dunsch and S. Yang, Small **3**, 1298 (2007).
[26] H. Shinohara, Rep. Prog. Phys. **63**, 843 (2000).
[27] D. S. Bethune, R. D. Johnson, J. R. Salem, M. S. Devries, and C. S. Yannoni, Nature (London) **366**, 123 (1993).
[28] M. Treier, P. Ruffieux, R. Fasel, F. Nolting, S. Yang, L. Dunsch, and T. Greber, Phys. Rev. B **80**, 081403 (2009).
[29] A. A. Popov and L. Dunsch, J. Am. Chem. Soc. **130**, 17726 (2008).

[30] M. Feng, J. Lee, J. Zhao, J. T. Yates, and H. Petek, J. Am. Chem. Soc. **129**, 12394 (2007).
[31] S. Stevenson, G. Rice, T. Glass, K. Harich, F. Cromer, M. R. Jordan, J. Craft, E. Hadju, R. Bible, M. M. Olmstead, K. Maitra, A. J. Fisher, A. L. Balch, and H. C. Dorn, Nature (London) **401**, 55 (1999).
[32] S. F. Yang, M. Kalbac, A. Popov, and L. Dunsch, ChemPhysChem **7**, 1990 (2006).
[33] J. P. Perdew, K. Burke, and M. Ernzerhof, Phys. Rev. Lett. **77**, 3865 (1996).
[34] G. Kresse and J. Hafner, Phys. Rev. B **47**, 558 (1993).
[35] G. Kresse and J. Hafner, Phys. Rev. B **48**, 13115 (1993).
[36] G. Kresse and J. Hafner, Phys. Rev. B **49**, 14251 (1994).
[37] G. Kresse and D. Joubert, Phys. Rev. B **59**, 1758 (1999).
[38] D. B. Dougherty, P. Maksymovych, J. Lee, and J. T. Yates, Jr., Phys. Rev. Lett. **97**, 236806 (2006).
[39] D. B. Dougherty, P. Maksymovych, J. Lee, M. Feng, H. Petek, and J. T. Yates, Phys. Rev. B **76**, 125428 (2007).
[40] X. H. Lu, M. Grobis, K. H. Khoo, S. G. Louie, and M. F. Crommie, Phys. Rev. B **70**, 214109 (2004).
[41] X. H. Lu, M. Grobis, K. H. Khoo, S. G. Louie, and M. F. Crommie, Phys. Rev. Lett. **90**, 096802 (2003).
[42] B. R. Shi, X. S. Wang, H. J. Huang, S. H. Yang, W. Heiland, and N. Cue, J. Phys. Chem. B **105**, 11414 (2001).
[43] N. Lin, H. J. Huang, S. H. Yang, and N. Cue, Phys. Rev. B **58**, 2126 (1998).
[44] Y. Hasegawa, Y. Ling, S. Yamazaki, T. Hashizume, H. Shinohara, A. Sakai, H. W. Pickering, and T. Sakurai, Phys. Rev. B **56**, 6470 (1997).